ISSN 0027-1349, Moscow University Physics Bulletin, 2024, Vol. 79, No. 3, pp. 308–317. © Allerton Press, Inc., 2024.
Russian Text © The Author(s), 2024, published in Vestnik Moskovskogo Universiteta, Seriya 3: Fizika, Astronomiya, 2024, Vol. 79, No. 3, 2430201.

PHYSICS OF NUCLEI AND ELEMENTARY PARTICLES

New Version of the Experimental Setup for the Measurement of γ-Quantum Emission Cross Sections in Nuclear Reactions Induced by 14.1 MeV Neutrons

Yu. N. Kopatch[1], D. N. Grozdanov[1,2], N. A. Fedorov[1,3], T. Yu. Tretyakova[1,3,4], P. I. Kharlamov[1,4*], A. V. Andreev[1,3], G. Ahmedov[1,5], D. Berikov[1,6], S. Dabylova[1,6], Pr. K. Das[1,7], A. Kumar[1,8], G. V. Panpushik[3], I. N. Ruskov[1,2], I. A. Sirakov[2], V. R. Skoy[1], P. G. Filonchik[1,9], K. Hramco[1,10], and TANGRA Collaboration[1]

[1]*Joint Institute for Nuclear Research, Dubna, Moscow oblast, 141980 Russia*

[2]*Institute for Nuclear Research and Nuclear Energy, Bulgarian Academy of Sciences, Sofia, 1784 Bulgaria*

[3]*Faculty of Physics, Lomonosov Moscow State University, Moscow, 119991 Russia*

[4]*Skobeltsyn Institute of Nuclear Physics (SINP MSU), Lomonosov Moscow State University, Moscow, 119991 Russia*

[5]*Nuclear Research Department, Innovation and Digital Development Agency, Baku, AZ0100 Azerbaijan*

[6]*L.N. Gumilyov Eurasian National University, Astana, 010008 Republic of Kazakhstan*

[7]*Department of Physics, Pabna University of Science and Technology, Pabna, 6600 Bangladesh*

[8]*Department of Physics, Institute of Science, Banaras Hindu University, Varanasi, 221005 India*

[9]*Moscow Institute of Physics and Technology, Dolgoprudny, Moscow oblast, 141701 Russia*

[10]*Institute of Chemistry of Moldova Academy of Science, Chisinau, MD-2028 Republic of Moldova*

Received December 28, 2023; revised February 19, 2024; accepted February 24, 2024

Abstract—Within the TANGRA project framework, a new experimental setup has been constructed for the measurement of cross sections of reactions (n, X, γ) in the interaction of 14.1 MeV neutrons with nuclei. The facility has a special feature: the use of the tagged neutron method. This method enables efficient separation of background and useful events, as well as accurate tracking of the neutron flux. Test measurements were performed on ^{28}Si, ^{12}C, and ^{16}O nuclei, and the results showed satisfactory agreement with available experimental data. This paper presents the features of the setup design and the methodology for processing the obtained experimental data.

Keywords: tagged neutron method, neutron-nuclear reactions, neutron scattering, gamma-spectrometry, HPGe detector

DOI: 10.3103/S0027134924700437

INTRODUCTION

Nuclear-physical methods for monitoring the composition of various materials, substances, and environments using neutrons are crucial for solving various scientific and applied problems. The development of convenient, compact neutron generators based on reactions involving light nuclei has expanded the use of fast neutron beams in a wide range of applied tasks. These include elemental analysis in industry [1, 2], the search for dangerous substances in security, exploration of oil, gas, and ore deposits, and determination of moisture in soils [3]. The modern environmental agenda has drawn attention to the task of creating mobile setups for determining the carbon content in soil [4, 5]. Research on nuclear power installations is particularly important: in recent years, due to the development of fourth-generation nuclear reactors [6], there has appeared a demand for a radical expansion and refinement of databases on the interaction of fast neutrons with matter.

Research on neutron-nuclear reactions, during which γ-quanta are emitted, is actively pursued in

*E-mail: pi.kharlamov@physics.msu.ru

large-scale projects. The most significant experiments studying these reactions include nELBE [7] and GELINA [8]. In these projects, photoneuclear reactions on lead and uranium are used as the source of neutrons, respectively, and the spectrum of emitted neutrons ranges from hundreds of kilovolts to ~20 MeV. The application of time-of-flight techniques allows for the study of nuclear reactions across a wide range of incident neutron energies and to obtain energy dependences of their characteristics. The use of high-resolution γ-radiation detectors in these experiments has enabled the measurement of emission cross sections and the anisotropy values of γ-quanta for a large number of γ-transitions.

Another process widely used for generating fast neutrons, especially in compact sources, is the fusion reaction of deuterium and tritium:

$$d + t \to n + \alpha + 17.56\ \text{MeV}. \qquad (1)$$

As a result of this reaction, fluxes of fast neutrons with an energy of about 14.1 MeV are formed. For elemental analysis using the spectra of characteristic γ-radiation, databases of cross sections for the formation of γ-quanta in the interaction processes of neutrons with atomic nuclei are necessary. Currently, a significant amount of experimental data has been accumulated on reactions of the type $(n, X\gamma)$, where $X = n, p, d, \alpha$ at neutron energy of 14.1 MeV, with the most comprehensive source of information about these quantities being compilation [9]. However, it should be noted that the values of cross sections for some γ-transitions contained in the database, measured in different experiments at different times, can vary several times. Also, there is a current task of expanding the database volume by including new elements and isotopes.

Within the framework of the international TANGRA project [10], a facility based on the compact neutron generator ING-27 [11, 12] has been established at the Frank Laboratory of Neutron Physics of the Joint Institute for Nuclear Research (JINR, Dubna), with the capability of implementing the tagged neutron method (TNM) [13–15]. This method is based on the registration of α-particles formed in reaction (1), and the subsequent registration of coincident γ-quanta emitted during the deexcitation of the products of nuclear reactions:

$$A\,(n, X)B^* \xrightarrow{\gamma} B.$$

Determining the direction of the α-particles' ejection fixes the direction of the neutron's ejection as well, thus effectuating "tagging" of the neutron. The tagged neutron method (TNM) allows for a significant reduction in background influence and enhances the accuracy of experimental data. The use of a compact neutron generator facilitates easy modifications to the experimental setup and operation with detecting systems of various geometries. Previous studies investigated angular distributions of γ-quanta using a system of 18 BGO detectors in a ring geometry [16, 17], and a setup version with a detector made of high-purity germanium (HPGe) was created for determining the yields of γ-quanta without the capability of measuring cross sections [18, 19]. The main goal of this work is to create a setup for measuring cross sections of reactions $(n, X\gamma)$ with greater efficiency in registering γ-radiation and better energy resolution than the configuration previously used by us. In the new modification, we use two detectors made of ultrapure germanium to register γ-quanta. It is also worth noting that using the industrial neutron generator ING-27 as the source of neutrons introduces specific features into the experimental procedure, determines the geometric arrangement of the setup components, and requires specialized data processing procedures.

1. NEUTRON SOURCE AND IMPLEMENTATION OF THE TAGGED NEUTRON METHOD

The 14.1 MeV neutron generator is a compact deuteron accelerator to the energy range of 30–90 keV with a tritium-enriched target. The TANGRA experiment's ING-27 neutron generator is a serial product of Dukhov All-Russian Research Institute of Automation. The sealed generator housing contains an ion source, a focusing system, a titanium target enriched with tritium, and a semiconductor position-sensitive α-particle detector.

Typical parameters of the ING-27 generator:

1. neutron flux: from 5×10^7 s^{-1} at the beginning of service life to 2.5×10^7 s^{-1} at the end;
2. continuous operation time: 8 h;
3. generator lifetime: 750 h;
4. tritium target activity: 7.4×10^{11} Bq;
5. accelerating voltage: 30–90 kV.

Neutron formation occurs as a result of the reaction $d + t \to \alpha + n$. The angular distribution of its products is close to isotropic. The kinetic energy of the deuterons is much less than that of the reaction products, therefore, the scattering angle of the α-particle and neutron is close to 180° in the lab frame. Registration of the α-particle by a position-sensitive detector allows determining the direction of the neutron's ejection corresponding to the

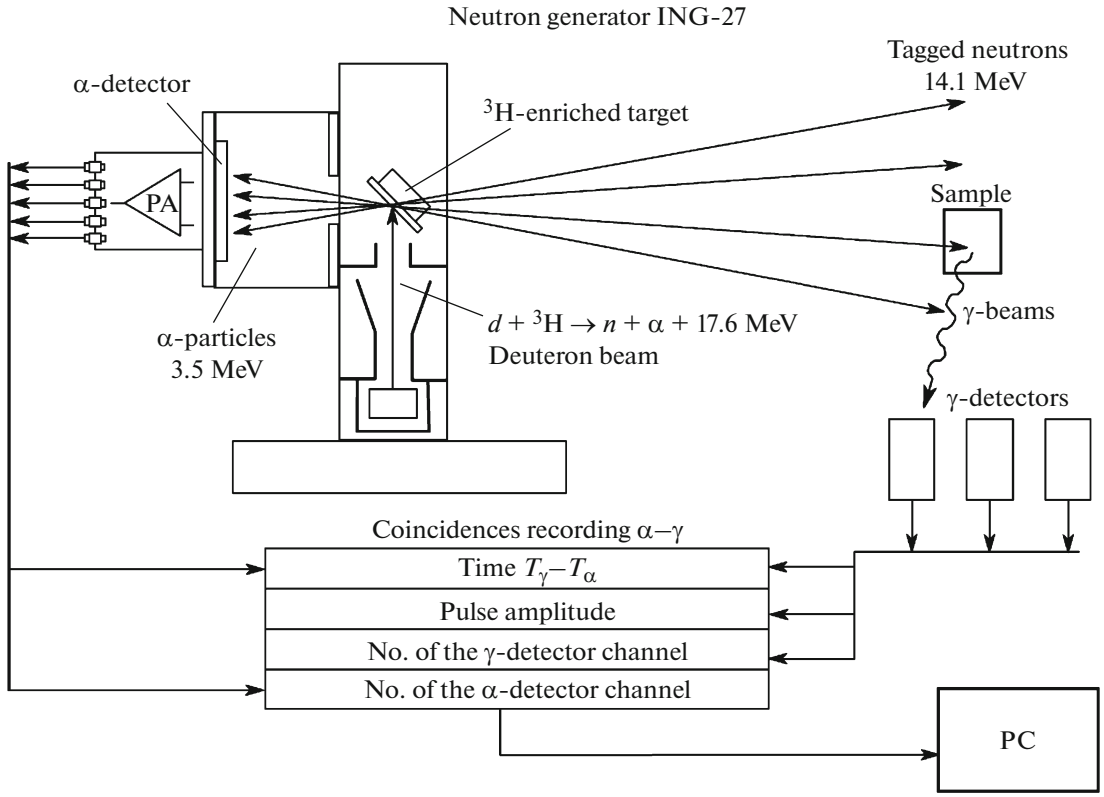

Fig. 1. Block diagram of the experiment using TNM.

α-particle, and gives a time stamp T_α, which serves as the "start" for determining the neutron's time of flight to the sample. Including the α-detector and detectors of secondary radiations in the coincidence scheme allows for the selection of events by time—the difference between the moment of secondary radiation registration T_γ and T_α. The block diagram of experiments using the TNM is shown in Fig. 1.

The use of a position-sensitive detector for the registration of α-particles allows obtaining several tagged neutron beams in one experiment. In this work, we used an α-detector with nine pixels, forming 9 tagged beams.

The energies of the tagged neutrons depend on the accelerating voltage and range from 14.0 to 14.3 MeV, with the centroid of distributions having values from 14.10 to 14.15 MeV (see Fig. 2).

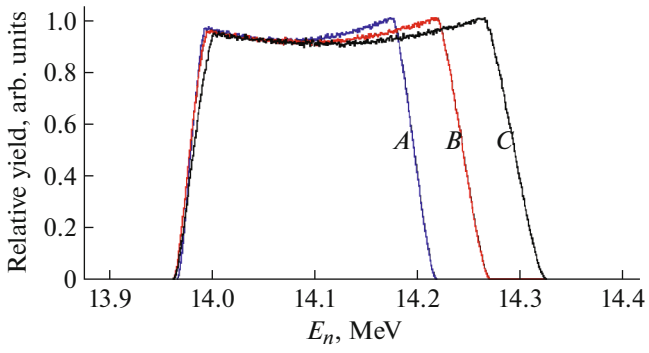

Fig. 2. Calculated neutron spectra for accelerating voltages of 40 (A), 60 (B), and 83 kV (C). The normalization is done on the peaks of the spectra.

2. OPTIMIZATION OF THE EXPERIMENTAL SETUP GEOMETRY

Previously, we used a setup configuration with a single HPGe detector [18]. Despite its successful application for studying neutron-nuclear reactions, the following disadvantages were noted:

1. risk of germanium detector degradation due to neutron irradiation stemming from its insufficient protection;

2. inability to use all available tagged beams.

Therefore, special attention was paid to eliminating these drawbacks when creating the new setup, and additional model calculations were conducted to minimize the absorption of γ-quanta in the sample.

The first step was the optimization of the geometry, composition, and thickness of the multicomponent

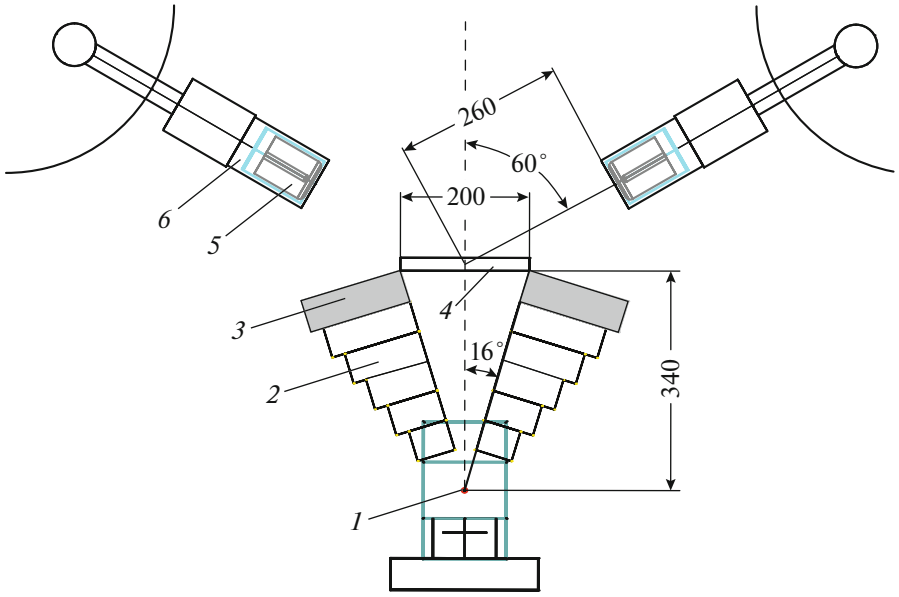

Fig. 3. Diagram of the modified setup based on HPGe detectors. *1*—ING-27, *2*—iron parts of the collimator, *3*—lead parts of the collimator, *4*—sample, *5*—HPGe crystal, *6*—detector housing. All dimensions are given in mm.

shadow shielding (collimator) using the GEANT4 software package. The shape of the shadow shielding, as well as the location of the target and detectors, was determined by the spatial distribution of the tagged neutron beams and was developed taking into account the following requirements:

1. tagged neutron beams should not enter the collimator;
2. the target area must cover all tagged neutron beams;
3. the distance from the target to the detectors should be minimal;
4. the neutron suppression factor in the collimator should be as high as possible;
5. the amount of secondary γ-quanta formed by the interaction of neutrons with the materials of the shielding and reaching the detectors should be minimal.

The optimal protection should provide minimal γ and neutron radiation doses in the germanium detector. The initial configuration of the shadow shielding assumed the presence of three different layers: polyethylene, slowing neutrons, a scattering layer of steel (iron), and lead, absorbing γ-radiation arising in iron during neutron-nuclear reactions [20].

Modelling was performed as follows: the total thickness of the shielding l_{sh} was fixed, after which the thicknesses of the polyethylene l_{PE}, steel l_{Fe}, and lead l_{Pb} layers were varied, such that $l_{\text{sh}} = l_{\text{PE}} + l_{\text{Fe}} + l_{\text{Pb}}$. Based on the calculations, the attenuation coefficient $k_{\text{sh}} = D_{\text{sh}}/D_0$ was determined, where D_{sh} is the total dose (including secondary γ-quanta) received by the detector with protection, and D_0 is the dose received by the detector without protection. Additionally, the calculation of the neutron dose attenuation coefficient $k^n_{\text{sh}} = D^n_{\text{sh}}/D^n_0$ was conducted. Experience from the previous setup indicated that the total thickness of the shielding l_{sh} should be no less than 20 cm [18]. Therefore, calculations were made for three values of l_{sh}: 20, 30, and 40 cm. Modelling results showed that polyethylene does not significantly reduce the absorbed dose of radiation. The optimal thickness of the lead component of the shielding is 5 cm. From these considerations, the following composition of the shadow shielding was chosen as a compromise between maximum protection for the germanium detectors and minimizing the distance between the detectors and the sample: $l_{\text{sh}} = 30$ cm, $l_{\text{Fe}} = 25$ cm, $l_{\text{Pb}} = 5$ cm. The calculated attenuation coefficients for such protection are $k_{\text{sh}} = 25$ and $k^n_{\text{sh}} = 41$. Figure 3 presents a diagram of the new version of the setup.

For γ-radiation detection, two ORTEC GMX60P4-83 ultrapure germanium detectors [21] with a relative efficiency of 60% and an energy resolution of 2.2 keV (full-width at half-maximum) at 1.33 MeV (^{60}Co) were used. It worsened to approximately 5 keV during the operation of the neutron generator. The neutron generator, shield, and detectors are mounted on a frame made of structural aluminum profile. The dimensions of the sample were

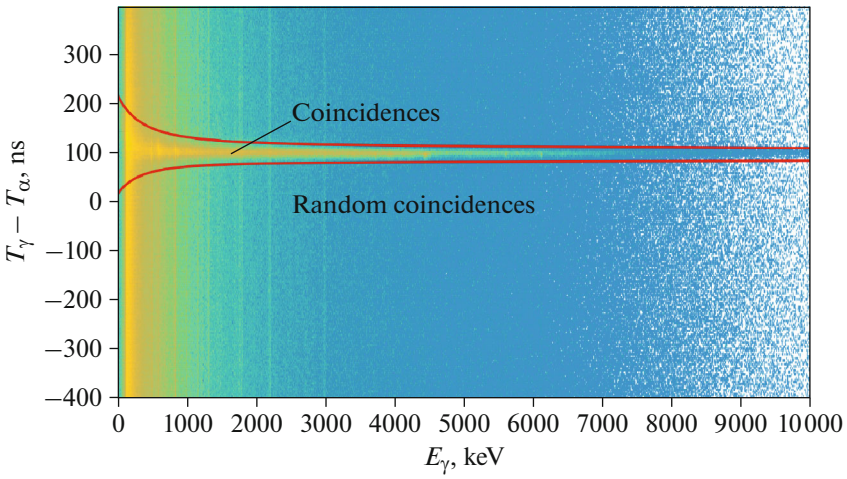

Fig. 4. Diagram: energy (E_γ)—time between the registration of the γ-quantum and its corresponding α-particle ($T_\gamma - T_\alpha$), formed as a result of reactions in the sample, with a highlighted coincidence window.

Table 1. Parameters of the used samples and characteristics of the conducted measurements

Sample	Density, g/cm^3	Type, dimension, cm^3	Measurement time, h	Tagged neutron flux, s^{-1}
C (nat)	1.74	Block $22 \times 22 \times 1.8$	5	4.4×10^5
SiO_2 (nat)	1.63	Container, $22 \times 22 \times 2$	18	6.4×10^4

chosen based on maximizing its coverage by tagged beams and minimizing the effects of γ-quantum absorption and multiple scattering of neutrons in the sample on the results obtained. Based on the modelling results, it was established that samples with dimensions 22×22 cm^2 meet these conditions; the thickness of the sample is determined based on optimizing the balance between absorption of γ radiation and maximizing the rate of statistics collection, and ranges from 1 to 4 cm. A container made of polyethylene with a wall thickness of 3 mm and the above-mentioned internal dimensions, filled with powder of the substance being studied, is used as the sample. Polyethylene (C_nH_{2n}) was chosen because it does not introduce significant distortions into the measured spectra, as the only reaction leading to the emission of γ-quanta is $^{12}C(n,n')$ with the excitation of a 4.4 MeV (2^+) level, which decays through a γ-transition to the ground state. The capture of fast neutrons by hydrogen nuclei is unlikely. Some samples may be manufactured directly in the form of blocks of the specified dimensions. The parameters of the samples and the characteristics of measurements with them are shown in Table 1.

3. PROCESSING OF EXPERIMENTAL DATA

In all experiments, data processing occurs in both on-line and off-line modes. An analog-to-digital converter (ADC), developed at JINR based on the ARTIX-7 FPGA and AD9656 ADC (16 bit, 125MSPS), is used for data collection, connected to a personal computer (PC) via a USB 3.0 interface. In on-line mode, the ADC processes pulses and groups them into coincidences (events). Data on the area, arrival time, and width of each registered pulse are transmitted to the PC. At a load of less than 2×10^4 pulses-per-second/channel, it is possible to transmit pulse oscillograms to the PC for subsequent off-line processing. The data obtained are saved in files for further analysis of amplitude and energy distributions. Below is an example of data analysis obtained from samples of carbon and silicon dioxide.

3.1. Selection of the Coincidence Spectrum

Data processing from germanium detectors begins with selecting windows on two-dimensional energy–time registration diagrams corresponding to reactions in the sample (Fig. 4). The window corresponds to coincidences of signals from the α- and HPGe detectors, considering the neutron flight time from the generator to the sample.

Figure 5 shows the time spectrum of events from the HPGe detector, which consists of a single peak on a flat background. The background, henceforth referred to as the "random coincidence background," is formed by γ-quanta from reactions of untagged neutrons with the structural elements of the setup and

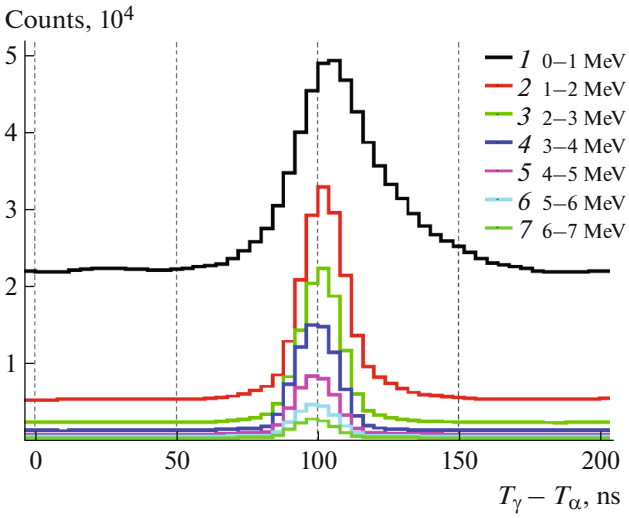

Fig. 5. Example of time spectra for the HPGe detector in different energy windows with a step of 1 MeV. Histograms are projections of Fig. 4 on the Y-axis.

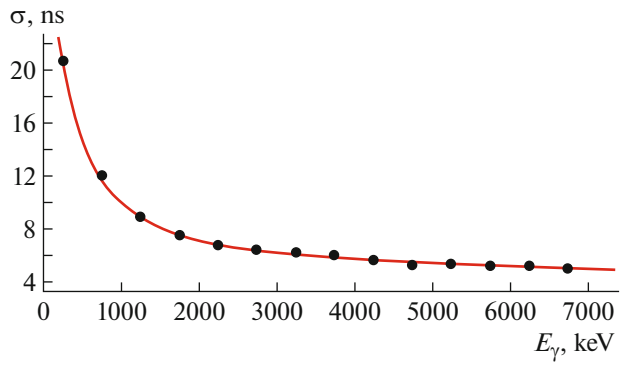

Fig. 6. Dependence of the full-width at half-maximum of the coincidence peak on the energy of the particle registered in the HPGe detector.

its surroundings. Events associated with reactions in the sample form a peak, whose position and dispersion depend on the energy of the γ-quanta.

The amplitude and dispersion of the coincidence peak in each of the time windows are determined both by the efficiency of the detector and by the scattering of γ-quanta by the sample's surroundings, which leads to an increase in the number of low-energy γ-quanta. The dependence of the full-width at half-maximum of the coincidence peak on energy is shown in Fig. 6.

In processing, events in the sample are selected as coincidence signals on energy–time registration diagrams (Fig. 4) within a window width of 6σ ($\pm 3\sigma$ from the centroid), henceforth referred to as "coincidences." From the "coincidence" spectrum, the random coincidence background is subtracted, and as a result, a distribution of "true coincidences" is

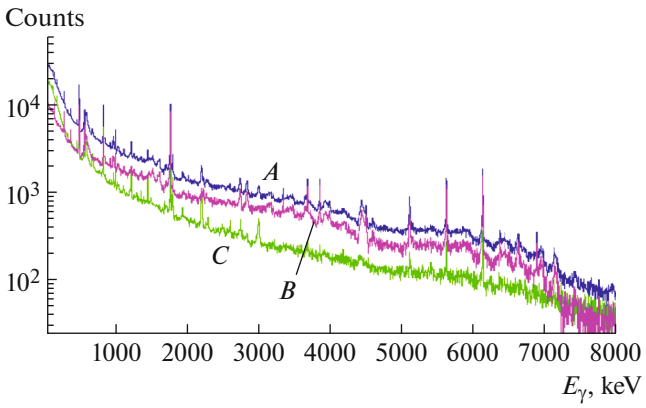

Fig. 7. Spectrum of true coincidences (B) compared with the spectrum in the coincidence window (A) and the spectrum of events outside the window (C) for the SiO_2 sample. All spectra are normalized to the width of the time window.

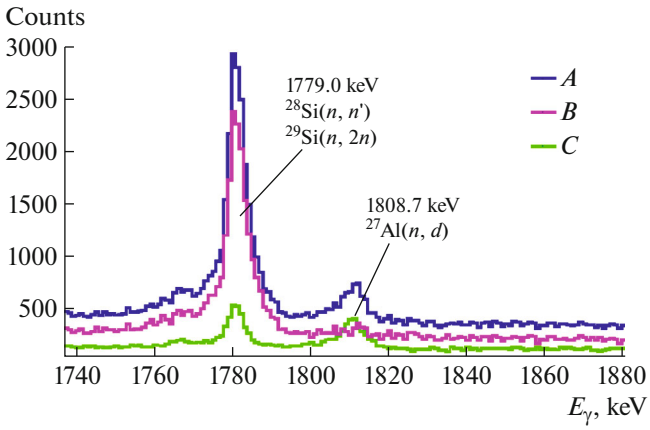

Fig. 8. Example of removing a background peak by subtracting the random coincidence spectrum. (A) spectrum in the coincidence window, (B) spectrum of true coincidences, (C) spectrum of events outside the coincidence window.

obtained, containing only events that occurred in the sample and its immediate surroundings. Energy spectra of γ-quanta are constructed for true coincidences (see Fig. 7).

The subtraction of the random coincidence background leads to significant suppression of background γ-peaks. This is demonstrated in Figs. 7 and 8, where the described procedure removes the background peak of γ-quanta at 1808.7 keV from the reaction ^{27}Al(n,d) in the setup frame.

The use of the tagged neutron method significantly reduces the number of background events in the processed spectra. Figure 9 shows a comparison of the spectrum without coincidences with the spectrum in the time window before and after subtracting the

Table 2. Results of test measurements of γ-radiation cross sections for ^{28}Si, ^{12}C, and ^{16}O compared with literature data [9]

		σ_γ, mb		
E_γ, keV	Reaction	TANGRA	Recommended values [9]	Range of experimental values [9]
1779.0	$^{28}\mathrm{Si}(n,n')^{28}\mathrm{Si}$, $^{29}\mathrm{Si}(n,2n')^{28}\mathrm{Si}$	350 ± 20	403 ± 20	$293 \pm 28 \ldots 488 \pm 70$
6129.9	$^{16}\mathrm{O}(n,n')^{16}\mathrm{O}$	113 ± 10	148 ± 10	$84 \pm 17 \ldots 179 \pm 22$
4438.9	$^{12}\mathrm{C}(n,n')^{12}\mathrm{C}$	175 ± 6	187 ± 5	$121 \pm 8 \ldots 440 \pm 80$

random coincidence spectrum for an experiment on a carbon target. The number of events in the region outside the γ-peaks (100–3300 keV) is suppressed by a factor of 67.

3.2. Detector Efficiency

For calculating cross sections determined by the areas of photopeaks, it is necessary to consider the detector's efficiency, the absorption of γ-quanta by the sample material, and the coverage of the sample by the neutron beam. Since the γ-quantum emission area has finite dimensions, experimental determination of the full efficiency of the detector system presents a significant challenge. The calculated distribution of reactions (centroids of tagged neutron beams) across the sample for all neutron beams is shown in Fig. 10.

To take into account the finite dimensions of the γ-quantum emission area, a correction was made

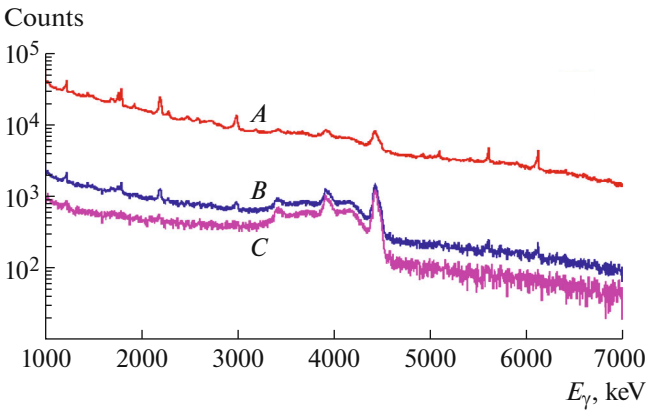

Fig. 9. Comparison of the "no coincidence" spectrum (A) with coincidence spectra in the peak window on a carbon target before (B) and after (C) subtracting the random coincidence spectrum.

to the procedure for estimating the γ-detector's efficiency. Indeed, for a point source with number i, one can write:

$$N_{i\gamma} = N_{i0}\, \varepsilon_i\, \kappa_i, \tag{2}$$

where $N_{i\gamma}$ and N_{i0} are the number of registered and emitted γ-quanta from point i, respectively, ε_i is the full efficiency of the detector for γ-quanta emitted from point i, κ_i is the absorption coefficient of γ-quanta in the sample. For an extended area consisting of a large number of points, formula (2) is transformed to:

$$N_\gamma = N_0 \sum_i \varepsilon_i \kappa_i p_i, \tag{3}$$

where N_γ is the number of registered γ-quanta, N_0 is the number of emitted γ-quanta, p_i is the probability of reaction at point i. An effective method of accounting for the nonpoint nature of the γ-quantum emission area, as well as their absorption in the sample material and the efficiency of the detector, is to model all these processes using the Monte Carlo method. In this case, it is possible to directly determine the efficiency of the detector ϵ as the ratio of the number of registered γ-quanta to the number of emitted ones:

$$\epsilon = \frac{N_\gamma}{N_0} = \sum_i \varepsilon_i \kappa_i p_i.$$

Calculations of the ϵ values for each combination of "tagged beam–pixel of α-detector" were performed using the GEANT4 software package. An example of the results of calculating ϵ compared with the value $\varepsilon = \sum_i \varepsilon_i p_i$ (without considering absorption in the sample) is shown in Fig. 11. It is evident that the self-absorption for the used sample is small. This fact minimizes the potential systematic error in data processing, arising from potentially incorrect data about the cross sections of nuclear reactions and assumptions about the shape of tagged beams used in modelling.

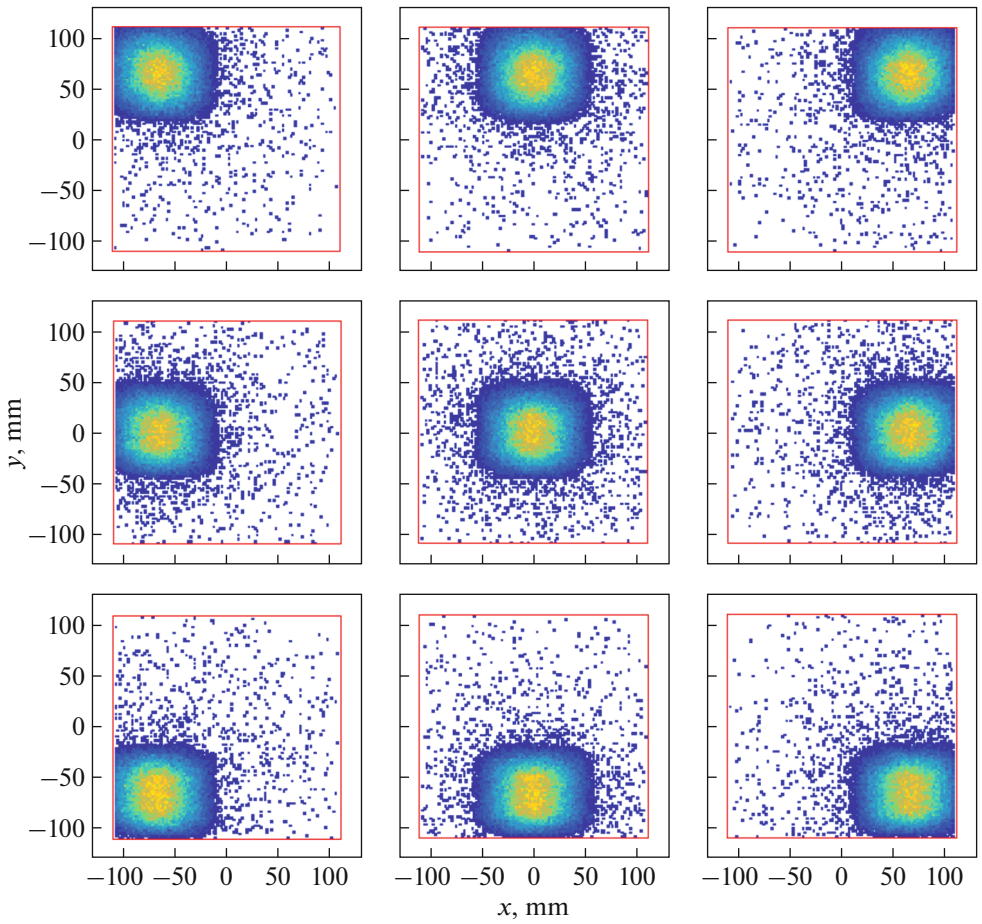

Fig. 10. Calculated distribution of interaction points of tagged neutrons with the sample material. The boundaries of the sample are shown with red lines. Coordinates are given in mm.

The cross sections for the formation of γ-quanta are calculated using the formula:

$$\sigma = \frac{N_\gamma M}{N_\alpha \chi_\alpha \rho_\alpha N_A d \epsilon \tau}, \qquad (4)$$

where N_α is the number of α-detector triggers, χ_α is the coverage factor of the target by the neutron beam needed to convert N_α to the number of neutrons hitting the target, ρ is the density of the sample, d is the average path traversed by neutrons in the target, M is the molar mass of the substance. The values χ_α and d are individual for each of the neutron beams and are calculated during modelling. The coefficient τ accounts for the dead time of the detector. To determine the dead time of germanium detectors, a series of measurements was conducted with calibration γ-sources and simultaneous operation of the neutron generator. The dead-time coefficient τ was determined as:

$$\tau(I) = \frac{C(I)}{C_0},$$

where $C(I)$ is the count rate at the γ-peak from the source at generator intensity I, and C_0 corresponds to the count rate with the generator turned off.

To verify the functionality of the assembled setup, experiments were conducted to measure the cross sections of γ-quantum emission in the most intense transitions in ^{28}Si, ^{12}C, and ^{16}O. The results are presented in Table 2. Our results were compared with available experimental data taken from [9]. This compilation provides results of various measurements made at neutron energies close to 14 MeV. Based on the analysis of their distributions, so-called recommended values of cross sections are estimated.

Our results are close to the values recommended in [9] and lie within the ranges of experimental data presented there. Full-scale measurements are expected to improve approximately threefold.

We have developed and tested a setup for measuring the cross sections of γ-quantum formation in reactions $(n, X\gamma)$, where $X \to n, p, d, \alpha$, induced by 14.1 MeV neutrons. A feature of the setup is the use of the portable ING-27 generator with the capability of using the tagged neutron method, which allows for effectively separating background

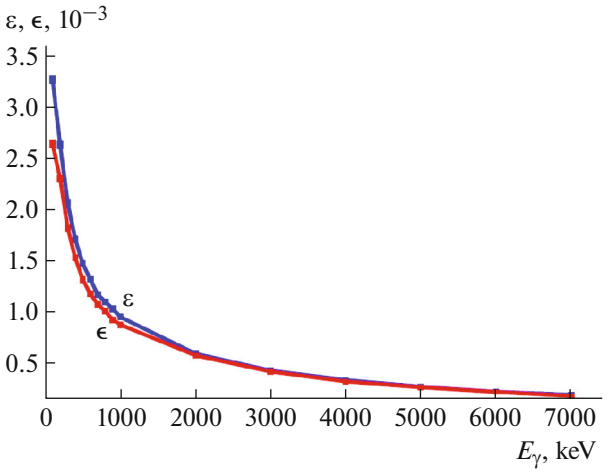

Fig. 11. Efficiency of the γ-quantum detector considering (ϵ) and excluding (ε) the absorption of γ-quanta in the carbon sample.

and useful events. To enhance the efficiency of registering γ-quanta of various energies, two large-volume HPGe γ-spectrometers with high energy resolution were used. To minimize radiation damage to γ-detectors and reduce their load from background γ-quanta, a two-layer shadow shielding was designed. A methodology for processing experimental data has been developed, enabling the effective isolation of events associated with reactions in the sample. During test measurements, cross sections for the most intense γ-transitions in nuclei of ^{28}Si, ^{12}C, and ^{16}O were obtained. The setup created will be used for systematic measurements of cross sections of γ-quantum emission in neutron-nuclear reactions on a range of elements to create a specialized database of neutron-nuclear data for 14.1 MeV neutrons, useful for applied and fundamental tasks.

FUNDING

This work was carried out with financial support from the Russian Science Foundation (grant no. 23-12-00239).

CONFLICT OF INTEREST

The authors of this work declare that they have no conflicts of interest.

REFERENCES

1. R. Grieken, A. Speecke, and J. Hoste, J. Radioanalytical Chem. **6**, 385 (1970). https://doi.org/10.1007/bf02513966
2. E. A. Razinkov, V. Yu. Aleksakhin, Yu. N. Rogov, and M. G. Sapozhnikov, Gorn. Zh., 51 (2022). https://doi.org/10.17580/gzh.2022.02.08
3. V. Valkovic, *14 MeV Neutrons: Physics and Applications* (CRC Press, Boca Raton, Fla., 2015). https://doi.org/10.1201/b18837
4. G. Yakubova, A. Kavetskiy, S. A. Prior, and H. A. Torbert, Appl. Radiat. Isot. **150**, 127 (2019). https://doi.org/10.1016/j.apradiso.2019.05.028
5. V. Yu. Alexakhin, E. A. Razinkov, Yu. N. Rogov, A. B. Sadovsky, M. G. Sapozhnikov, I. D. Dashkov, D. N. Grozdanov, Yu. N. Kopach, V. R. Skoy, and N. A. Fedorov, Phys. Part. Nucl. Lett. **19**, 717 (2022). https://doi.org/10.1134/s1547477122060024
6. G. Locatelli, M. Mancini, and N. Todeschini, Energy Policy **61**, 1503 (2013). https://doi.org/10.1016/j.enpol.2013.06.101
7. E. Altstadt, C. Beckert, H. Freiesleben, V. Galindo, E. Grosse, A. R. Junghans, J. Klug, B. Naumann, S. Schneider, R. Schlenk, A. Wagner, and F.-P. Weiss, Ann. Nucl. Energy **34**, 36 (2007). https://doi.org/10.1016/j.anucene.2006.11.005
8. D. Ene, C. Borcea, S. Kopecky, W. Mandelaers, A. Negret, and A. J. M. Plompen, Nucl. Instrum. Methods Phys. Res., Sect. A **618**, 54 (2010). https://doi.org/10.1016/j.nima.2010.03.005
9. S. P. Simakov, A. Pavlik, and H. Vonach, *Status of Experimental and Evaluated Discrete Gamma-Ray Production at En =14.5 MeV* (International Atomic Energy Agency, Vienna, 1998). https://www-nds.iaea.org/publications/indc/indc-ccp-0413/.
10. TANGRA Project, Frank Laboratory of Neutron Physics, https://flnp.jinr.int/ru/glavnaya/ustanovki/tangra-project-ru.
11. E. P. Bogolyubov, S. A. Korotkov, S. A. Krasnov, Yu. Presnyakov, and T. O. Khasaev, in *Proc. Int. Sci.-Tech. Conf. on Portable Neutron Generators and Technologies Based on Them* (VNIIA im. Dukhova, Moscow, 2005), p. 326.
12. V. M. Bystritskii, N. I. Zamyatin, V. G. Kadyshevskii, A. P. Kobzev, V. A. Nikitin, Yu. N. Rogov, M. G. Sapozhnikov, A. N. Sisakyan, and V. M. Vlasov, in *Proc. Int. Sci.-Tech. Conf. on Portable Neutron Generators and Technologies Based on Them* (VNIIA im. Dukhova, Moscow, 2005), p. 306.
13. I. N. Ruskov, Yu. N. Kopatch, V. M. Bystritsky, V. R. Skoy, V. N. Shvetsov, F.-J. Hambsch, S. Oberstedt, R. C. Noy, P. V. Sedyshev, D. N. Grozdanov, I. Zh. Ivanov, V. Yu. Aleksakhin, E. P. Bogolyubov, Yu. N. Barmakov, S. V. Khabarov, A. V. Krasnoperov, A. R. Krylov, J. Obhođaš, L. B. Pikelner, V. L. Rapatskiy, et al., Phys. Procedia **64**, 163 (2015). https://doi.org/10.1016/j.phpro.2015.04.022
14. V. M. Bystritsky, V. Valkovic, D. N. Grozdanov, A. O. Zontikov, I. Zh. Ivanov, Yu. N. Kopatch, A. R. Krylov, Yu. N. Rogov, I. N. Ruskov, M. G. Sapozhnikov, V. R. Skoy, and V. N. Shvetsov,

Phys. Part. Nucl. Lett. **12**, 325 (2015). https://doi.org/10.1134/s1547477115020089

15. V. M. Bystritsky, D. N. Grozdanov, A. O. Zontikov, Yu. N. Kopach, Yu. N. Rogov, I. N. Ruskov, A. B. Sadovsky, V. R. Skoy, Yu. N. Barmakov, E. P. Bogolyubov, V. I. Ryzhkov, and D. I. Yurkov, Phys. Part. Nucl. Lett. **13**, 504 (2016). https://doi.org/10.1134/s154747711604004x
16. D. N. Grozdanov, N. A. Fedorov, V. M. Bystritski, Yu. N. Kopach, I. N. Ruskov, V. R. Skoy, T. Yu. Tretyakova, N. I. Zamyatin, D. Wang, F. A. Aliev, C. Hramco, A. Gandhi, A. Kumar, S. Dabylova, E. P. Bogolubov, and Yu. N. Barmakov, Phys. At. Nucl. **81**, 588 (2018). https://doi.org/10.1134/s106377881805006x
17. N. A. Fedorov, T. Yu. Tret'yakova, D. N. Grozdanov, V. M. Bystritskii, Yu. N. Kopach, I. N. Ruskov, V. R. Skoi, N. I. Zamyatin, D. Van, F. A. Aliev, K. Khramko, A. Gandi, A. Kumar, M. G. Sapozhnikov, Yu. N. Rogov, E. A. Razinkov, and S. Dabylova, Uchen. Zap. Fiz. Fak. Mosk. Univ., No. 2, 1820205 (2018).
18. N. A. Fedorov, D. N. Grozdanov, Yu. N. Kopatch, T. Yu. Tretyakova, I. N. Ruskov, V. R. Skoy, I. D. Dashkov, F. A. Aliyev, S. Dabylova, C. Hramco, A. Kumar, A. Gandhi, D. Wang, E. P. Bogolyubov, and D. I. Yurkov, Eur. Phys. J. A **57**, 194 (2021). https://doi.org/10.1140/epja/s10050-021-00503-x
19. D. Grozdanov, N. Fedorov, S. Dabylova, Yu. Kopatch, I. Ruskov, V. Skoy, T. Tretyakova, C. Hramco, P. Kharlamov, G. Pampushik, P. Filonchik, and A. Andreev, Chin. Phys. C (2023). https://doi.org/10.1088/1674-1137/ad147e
20. V. M. Bystritsky, V. Valkovic, D. N. Grozdanov, A. O. Zontikov, I. Zh. Ivanov, Yu. N. Kopatch, A. R. Krylov, Yu. N. Rogov, I. N. Ruskov, M. G. Sapozhnikov, V. R. Skoy, and V. N. Shvetsov, Phys. Part. Nucl. Lett. **12**, 325 (2015). https://doi.org/10.1134/s1547477115020089
21. ORTEC GMX Series Coaxial HPGe Detector Product Configuration Guide, https://www.ortec-online.com/-/media/ametekortec/brochures/g/gamma-x-a4.pdf?la=en revision=420cd7bb-9d75-485c-80a2-acaaccdf8197.